Journal of Mathematical Imaging and Vision
https://doi.org/10.1007/s10851-022-01129-4

Nonlocal Adaptive Biharmonic Regularizer for Image Restoration

Ying Wen[1] · Luminita A. Vese[2] · Kehan Shi[3] · Zhichang Guo[1] · Jiebao Sun[1]

Received: 21 March 2021 / Accepted: 19 October 2022

Abstract
In this paper, we propose a nonlocal adaptive biharmonic regularization term for image restoration, combining the advantages of fourth-order models (preserving slopes) and nonlocal methods (preserving textures). Besides the image deblurring and denoising, we apply the proposed nonlocal adaptive biharmonic regularizer to image inpainting, and a weight matrix normalization method is developed to cover the shortage of information loss of the nonlocal weight matrix and accelerate the inpainting process. The existence and uniqueness of the solution are proved. The mathematical property such as mean invariance is discussed. For the numerical solution, we employ the L^2 gradient descent and finite difference methods to design explicit and semi-implicit schemes. Numerical results for image restoration are shown on synthetic images, real images, and texture images. Comparisons with local fourth-order models, nonlocal second-order models, and other state-of-the-art methods are made, which help to illustrate the advantages of the proposed model.

Keywords Nonlocal method · Fourth-order · Image deblurring and denoising · Image inpainting

1 Introduction

Image restoration has always been an essential and challenging task in the fields of image processing and computer vision. The image degradation model is

$$f = Hu + n, \tag{1}$$

where H is a linear operator accounting for some blurring, subsampling, or missing pixels, n is additive noise, f is the observed image, and u is the image we want to restore. The restoration problem (1) is ill-posed. Image deblurring and denoising is a problem of recovering the image from the blurred image with noise pollution [8,12,16,35,45,49], which is the fundamental problem generally arising in the field of image processing with several applications. Image inpainting [4,13,30,38,43,46,53] is one of the common restoration tasks. It is the process of reconstructing lost or corrupted parts of an image, which is a technique of removing undesirable objects from the image without leaving traces like artifacts ghosts [15]. An excellent inpainting method must restore coherently both texture and structure components of the image. Usually, the undesired object we want to remove is scratch, texture, signature, mask, block, noise, etc.

Until now, there are a variety of methods developed to deal with the restoration problem in the variational setting. Rudin, Osher, and Fatemi proposed the total variation

This paper is an extension of the published conference paper [48]. Based on the conference paper [48], we add the theoretical analysis of the proposed nonlocal adaptive biharmonic model and the application of image inpainting, and improve the experimental comparison in this paper. The other parts are the same as the conference paper except for some structural adjustments.
Ying Wen thanks Professor Andrea Bertozzi for hosting her for studying at UCLA from September 2019 to October 2020. The authors would like to thank all anonymous referees for their valuable comments and suggestions, and thank Jianlou Xu for sharing their source code.

✉ Zhichang Guo
mathgzc@hit.edu.cn

Ying Wen
wenyinghitmath@gmail.com

Luminita A. Vese
lvese@math.ucla.edu

Kehan Shi
kshi@cjlu.edu.cn

Jiebao Sun
sunjiebao@hit.edu.cn

[1] Harbin Institute of Technology, Harbin 150001, China

[2] University of California, Los Angeles, CA 90024, USA

[3] Department of Mathematics, China Jiliang University, Hangzhou 310018, China

Published online: 10 November 2022

regularization [42] which is remarkably effective at simultaneously preserving edges while smoothing away noise in flat regions, and it is widely applied to various research fields of computer vision. Perona and Malik proposed a partial differential equation based model for image denoising [41] which consists of a forward–backward diffusion process controlled by a diffusion coefficient to smooth noise and preserve edges. To overcome the staircase effect of edge-preserving second-order partial differential equation methods, fourth-order equations for image denoising have been employed. We mention the earlier work of Chambolle and Lions [7], of Chan, Marquina, and Mulet [9], of You and Kaveh [52], of Lysaker et al. [36], and of Hajiaboli [19,20]. These models can better preserve smooth regions and ramps, thus diminishing the staircase effect. Kim et al. [27] proved that the solution of a fourth-order PDE model converges to a piecewise harmonic function under a specific condition. Some diffusion-based methods [3,29,43] inpaint images by propagating higher-order derivatives of local pixel intensity continuously along the lines of equal intensity values, toward the interior of the missing region. Diffusion-based inpainting performs well in achieving consistent intensity. These image restoration methods are based on local image operators. However, texture is nonlocal in nature and requires nonlocal information for efficient image restoration.

Buades, Coll, and Morel proposed the nonlocal means filter by weighted averaging the nonlocal similar pixels [6]. The similarity between pixels is measured by the similarity between their patches. Following the nonlocal means filter and inspired by the gradient and Laplacian on graphs, Gilboa and Osher [17,18] defined the nonlocal gradient, nonlocal Laplacian, etc., and extended the nonlocal method to the variational framework. They formulated the nonlocal total variation regularization for image denoising, inpainting, anomaly detection, and image-texture separation.

The variational nonlocal framework is widely utilized for various image processing tasks. Based on the Mumford-Shah framework, Jung et al. [24] extended the Ambrosio-Tortorelli [1] and Shah [44] approximations to the nonlocal version, and applied it to color image restoration. In the work of Lou et al. [34], the authors extended the nonlocal total variation model to image restoration (simultaneous denoising and deblurring). Liu et al. [33] employed the nonlocal total variation as the regularization and Gabor functions as the fidelity for image denoising and decomposition. Nie et al. [39] proposed the nonlocal total variation-based variational model of complex-valued fourth-order tensor data for the polarimetric synthetic aperture radar data speckle reduction. For despeckling of synthetic aperture radar images, based on the variational nonlocal framework and statistical properties, Ma et al. [37] proposed two models from both transformed domain and original domain with different similarity measurements. Besides noise removal, nonlocal models could better preserve details and repetitive structures such as texture, edges, and polarimetric scattering characteristics. For image dehazing, Liu et al. [31] proposed the nonlocal total variation-based model with an adaptive function to overcome halo effects and artifacts amplification. Jin et al. [23] proposed an adaptive nonlocal total variation model by replacing the constant regularization parameter with an adaptive function that could recognize flat areas and non-flat areas. We also mention the other nonlocal first-order variation-based works [22,28]. Corresponding to the local case, the nonlocal p-Laplacian has been proposed for image restoration to preserve fine structures [21,25,26].

Due to the nonlocal property, the fractional-order derivative is suitable to deal with edges and textures. Recently, fractional derivative-based variational and diffusion equation models were proposed for image restoration. The fractional-order TV-L^2 model was constructed for image denoising [10] and numerically obtained improved denoising results over the total variation model [42]. Zhang and Chen [54] studied a total fractional-order variational model with nonhomogeneous boundary conditions for image restoration, and analyzed the theoretical properties. Yao et al. [51] proposed an adaptive anisotropic fractional diffusion equation for multiplicative noise removal, and a gray level indicator was introduced for the construction of the diffusion coefficient. Based on the fractional Laplacian, researchers designed corresponding diffusion equations for image processing [2,32].

Here, we propose a nonlocal fourth-order regularizer for image restoration, which can be seen as a nonlocal version of the biharmonic operator. Also, isotropic and anisotropic versions are considered. Compared with the nonlocal harmonic model, the nonlocal biharmonic model can better preserve slopes and maintain contrast. In the anisotropic case, adaptive coefficients, depending on the input image, help to preserve edges while smoothing out homogeneous regions. We apply the regularizer to image denoising, image deblurring in the presence of Gaussian noise (image deblurring and denoising), and image inpainting. For the gradient descent flow of the functionals, the uniqueness and existence of the solution are proved. We also prove the mean value invariance of the proposed image denoising model. In terms of the numerical implementation, two finite difference schemes, explicit and semi-implicit are investigated. A weight matrix normalization is developed to accelerate the inpainting process by removing the weight value of each pixel itself and normalizing each row of the weight matrix. Experiments of restoration of synthetic, natural, and texture images show the effectiveness of our models.

The paper is organized as follows: In Sect. 2, we introduce the background of high-order models and nonlocal methods. The nonlocal adaptive biharmonic model is proposed in Sect. 3, and also we apply the proposed regularizer to image deblurring and denoising and image inpainting. In

Sect. 4, the theoretical analysis of the proposed model is discussed. Finite difference schemes are designed for numerical implementation in Sect. 5, and also the construction details of the weight matrix are presented. In Sect. 6, experiments for image restoration of our method are shown, and the proposed method is compared with other methods. Finally, the work is summarized in Sect. 7.

2 Background

For the image restoration problem, let $\Omega \subset \mathbb{R}^2$ be the image domain, $f : \Omega \to \mathbb{R}$ the observed image, and $u : \Omega \to \mathbb{R}$ the restored image.

2.1 Local Fourth-Order Models

We recall several local fourth-order models previously introduced in [36,52].

The You-Kaveh (YK) regularizer [52] is

$$E^{YK}(u) = \int_\Omega g(|\Delta u|)\mathrm{d}x,$$

where the authors require $g(\cdot) \geq 0$, $g'(\cdot) > 0$, and its corresponding time-dependent Euler–Lagrange equation is

$$\frac{\partial u}{\partial t} = -\Delta\left(g'(|\Delta u|)\frac{\Delta u}{|\Delta u|}\right) = -\Delta(c(|\Delta u|)\Delta u).$$

Usually, set $c(\cdot) = \frac{1}{1+(\cdot/k)^2} = g'(\cdot)$ and k is a modulatory parameter, which is the edge-preservation function from [41] (the independent variable being now $|\Delta u|$ instead of $|\nabla u|$).

The Lysaker–Lundervold–Tai (LLT) regularizer [36] minimizes the total variation norm of ∇u, and it is

$$E^{LLT}(u) = \int_\Omega (|u_{x_1x_1}| + |u_{x_2x_2}|)\mathrm{d}x.$$

These fourth-order models encourage piecewise planar solutions [52]. Thus, these models can preserve edges without the staircase effect.

2.2 Nonlocal Operators

Nonlocal methods are well adapted to texture preservation and denoising. Referred to [17,18], we first review nonlocal differential operators. The nonlocal gradient vector $\nabla_w u(x) : \Omega \to \Omega \times \Omega$, is defined by

$$(\nabla_{NL}u)(x, y) := (u(y) - u(x))\sqrt{w(x, y)},$$

where $w : \Omega \times \Omega \to \mathbb{R}$ is a nonnegative and symmetric weight function, such as

$$w(x, y) = \exp\left\{-\frac{G_\sigma * (\|u(x + \cdot) - u(y + \cdot)\|^2)(0)}{2h^2}\right\}, \tag{2}$$

where $G_\sigma = \frac{1}{2\pi\sigma^2}e^{-\frac{\|x\|^2}{2\sigma^2}}$. And the magnitude of nonlocal gradient at $x \in \Omega$ is

$$|\nabla_{NL}u|(x) = \sqrt{\int_\Omega (u(y) - u(x))^2 w(x, y)\mathrm{d}y}.$$

The nonlocal divergence $\mathrm{div}_{NL}\mathbf{v} : \Omega \times \Omega \to \Omega$ of the vector $\mathbf{v} : \Omega \times \Omega \to \mathbb{R}$ is defined as the adjoint of the nonlocal gradient

$$(\mathrm{div}_{NL}\mathbf{v})(x) := \int_\Omega (v(x, y) - v(y, x))\sqrt{w(x, y)}\mathrm{d}y.$$

The nonlocal Laplacian $\Delta_{NL}u : \Omega \to \mathbb{R}$ of u can be defined by

$$\begin{aligned}\Delta_{NL}u(x) &:= \frac{1}{2}\mathrm{div}_{NL}(\nabla_{NL}u(x)) \\ &= \int_\Omega (u(y) - u(x))w(x, y)\mathrm{d}y.\end{aligned}$$

2.3 Variational Nonlocal Methods

Based on the above nonlocal operators, the nonlocal harmonic (NLH) regularization [17] is

$$E^{\mathrm{NLH}}(u) = \int_\Omega |\nabla_{NL}u|^2\mathrm{d}x,$$

and the associated time-dependent Euler–Lagrange equation is

$$\frac{\partial u}{\partial t} = \int_\Omega (u(y) - u(x))w(x, y)\mathrm{d}y,$$

and it can also be expressed as $\frac{\partial u}{\partial t} = \Delta_{NL}u$.

The nonlocal total variation (NLTV) regularization [18] is

$$E^{\mathrm{NLTV}}(u) = \int_\Omega |\nabla_{\mathrm{NL}}u|\mathrm{d}x,$$

and the associated time-dependent Euler–Lagrange equation is

$$\begin{aligned}\frac{\partial u}{\partial t} &= \int_\Omega (u(y) - u(x))w(x, y) \\ &\quad \left(\frac{1}{|\nabla_{\mathrm{NL}}u(x)|} - \frac{1}{|\nabla_{\mathrm{NL}}u(y)|}\right)\mathrm{d}y,\end{aligned}$$

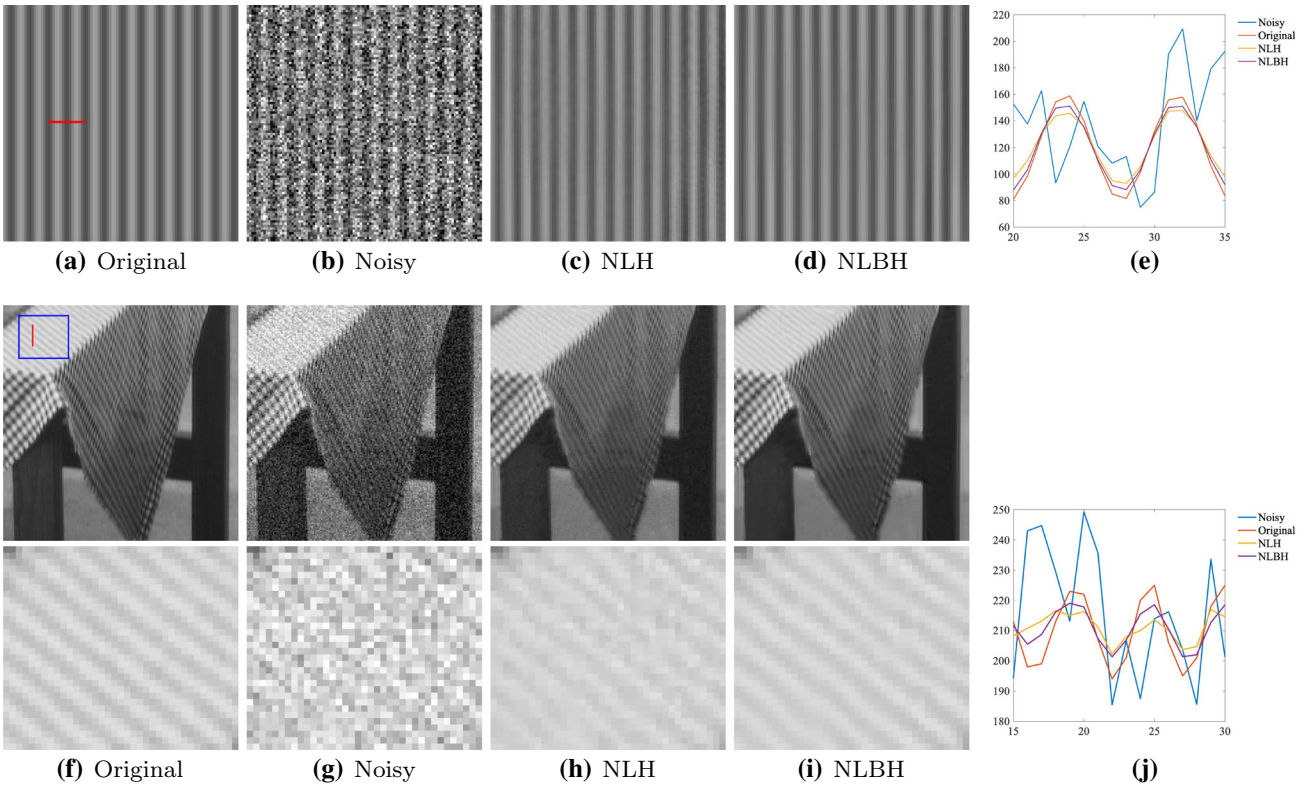

Fig. 1 Compared with the NLH model, the proposed nonlocal biharmonic model can better preserve slopes and maintain contrast. **e** Signals at the red line of **a**. **j** Signals at the red line of **f** (Color figure online)

which can also be expressed as $\frac{\partial u}{\partial t} = \mathrm{div}_{\mathrm{NL}}\left(\frac{\nabla_{\mathrm{NL}} u}{|\nabla_{\mathrm{NL}} u|}\right)$.

3 The Proposed Model

Inspired by the local fourth-order models and the nonlocal gradient and Laplacian, we propose the following nonlocal adaptive biharmonic regularizer for image restoration,

$$E(u) = \int_{\Omega} \alpha(f) |\Delta_{\mathrm{NL}} u|^2 \mathrm{d}x, \tag{3}$$

where $|\Delta_{\mathrm{NL}} u(x)| = |\int_{\Omega}(u(y) - u(x))w(x, y)\mathrm{d}y|$, $\alpha(f)$ is an adaptive coefficient function to distinguish edges and smooth areas and thus to adaptively guide the image restoration process.

3.1 Choices of α

In the following, several choices of $\alpha(f)$ are given.

The first one is $\alpha(f) = 1$. The model (3) is isotropic, and the regularization term becomes a nonlocal biharmonic (NLBH) model. Fourth-order linear diffusion damps oscillations at high frequencies much faster than second-order diffusion [5]. At the same time, different from second-order methods, fourth-order methods can efficiently preserve slopes and creases in the image. In Fig. 1, compared with the NLH model, the contrast of the NLBH denoising results are higher (Fig. 1e, j). It verifies the slope preservation property of the NLBH model. We also illustrate that the NLBH model has better contrast maintenance than the NLH model by the following deduction. The explicit scheme of the NLH equation with time step τ is

$$(u_{\mathrm{NLH}})_i^{n+1} = u_i^n + \tau \Delta_{\mathrm{NLd}} u_i^n.$$

The time-dependent Euler–Lagrange equation of the proposed NLBH model is

$$\frac{\partial u}{\partial t} = -\Delta_{\mathrm{NL}}(\Delta_{\mathrm{NL}} u),$$

and when the time step is τ^2, its explicit scheme is

$$\begin{aligned}(u_{\mathrm{NLBH}})_i^{n+1} &= u_i^n - \tau^2 \Delta_{\mathrm{NLd}}(\Delta_{\mathrm{NLd}} u_i^n) \\ &= u_i^n - \tau \Delta_{\mathrm{NLd}}(u_{\mathrm{NLH}})_i^{n+1} + \tau \Delta_{\mathrm{NLd}} u_i^n \\ &= (u_{\mathrm{NLH}})_i^{n+1} - \tau \Delta_{\mathrm{NLd}}(u_{\mathrm{NLH}})_i^{n+1} \\ &= (u_{\mathrm{NLH}})_i^{n+1} + ((u_{\mathrm{NLH}})_i^{n+1} - (u_{\mathrm{NLH}})_i^{n+2}).\end{aligned}$$

The above equation shows that the NLBH model can compensate for the differences caused by the NLH model (smoothed features, $((u_{\mathrm{NLH}})_i^{n+1}-(u_{\mathrm{NLH}})_i^{n+2})$), which means that NLBH can better preserve structure and obtain finer results. It is consistent with the experiments in Fig. 1.

The second one is

$$\alpha(f)=\frac{1}{1+|\nabla f_\sigma|^2/k^2}, \tag{4}$$

where k is a modulatory parameter, and $f_\sigma = G_\sigma * f$ with $G_\sigma = 1/(2\pi\sigma^2)\exp\{-\|x\|^2/(2\sigma^2)\}$ is a smoothed version of f. Using eq. (4), model (3) becomes anisotropic, and $\alpha(f)$ provides a guidance for the degree of diffusion. With coefficient (4), the functional (3) is a nonlocal adaptive biharmonic (NLABH) model. We use f_σ to first roughly remove the noise and then utilize the gradient ∇f_σ as an edge detector. Thus, $\alpha(f)$ has the ability of distinguishing edges and smooth areas of the original image. From the coefficient (4), $\alpha(f)\in[0,1]$. On or near edges, $|\nabla f_\sigma|$ is large and thus $\alpha(f)$ is small approaching 0. On the contrary, on flat areas or away from edges, $|\nabla f_\sigma|$ is small and $\alpha(f)$ is large approaching 1. Using this coefficient (4) in the proposed high-order functional (3), we have that $\alpha(f)$ induces less diffusion when $|\nabla f_\sigma|$ is large for preserving structures, and bigger diffusion when $|\nabla f_\sigma|$ is small for smoothing out the noise. Besides, we can also employ the nonlocal gradient to guide the diffusion,

$$\alpha(f)=\frac{1}{1+|\nabla_{\mathrm{NL}} f_\sigma|^2/k^2}. \tag{5}$$

We verify the effectiveness of the adaptive coefficient for the nonlocal methods through the following denoising experiments. The nonlocal adaptive harmonic (NLAH) model is

$$\frac{\partial u}{\partial t}=\frac{1}{2}\mathrm{div}_{NL}(\alpha_{NL}(f)\nabla_{NL}u)+\lambda(f-u).$$

And the comparison experiments are displayed as follows, and all of parameters are tuned for best restoration performance. We show the denoising results in Fig. 2, and the PSNR [14] values between the noisy image and restored image in Table 1. In the PSNR measurement, the adaptive models are better than the models without adaptive coefficient.

3.2 Image Deblurring and Denoising

The image deblurring and denoising degradation model is

$$f=Ku+n,$$

where $K: L^2(\Omega)\to L^2(\Omega)$ models the blur kernel which is a linear and continuous operator, $\Omega\subset\mathbb{R}^2$ is the image domain, and f is the given noisy blurred image. Note, if the blur kernel is identity matrix, it represents the image denoising problem. For image deblurring and denoising problem, if the noise n is the Gaussian noise, the data fidelity term is

$$F^{\mathrm{Gau}}=\frac{\lambda}{2}\int_\Omega (f-Ku)^2\mathrm{d}x,$$

where $\lambda>0$ is the parameter to balance the regularization term and data fidelity term. The functional we proposed for image deblurring and denoising problem is

$$E(u)=\frac{1}{2}\int_\Omega \alpha(f)|\Delta_{NL}u|^2\mathrm{d}x+\frac{\lambda}{2}\int_\Omega (f-Ku)^2\mathrm{d}x. \tag{6}$$

The corresponding Euler–Lagrange equation associated with eq. (6), in a time-dependent fashion, is

$$\frac{\partial u}{\partial t}=-\Delta_{NL}(\alpha(f)\Delta_{NL}u)+\lambda K^*(f-Ku), \tag{7}$$

with initial condition $u(x,0)=f(x), x\in\Omega$, where K^* is the adjoint operator of K.

Note that, the anisotropic adaptive coefficient functions work better than the isotropic one for image deblurring and denoising, because they can adaptively guide the image restoration process by distinguishing edges and smooth areas.

3.3 Image Inpainting

The nonlocal-based methods are good at texture preservation. At the same time, high-order methods have the advantage of preserving weak slopes. Thus, we employ the proposed nonlocal adaptive biharmonic model for image inpainting. The mathematical model of image inpainting is

$$f=u \quad \text{on} \quad \Omega-D,$$

where D is the damaged region in the image.

The data fidelity term for image inpainting is

$$F^{\mathrm{Inp}}=\frac{\lambda}{2}\int_\Omega \chi_{\Omega-D}(x)(f-u)^2\mathrm{d}x,$$

where $\chi_{\Omega-D}$ is a characteristic function on Ω (i.e., $\chi_{\Omega-D}(x)=1$, if $x\in\Omega-D$, 0 otherwise), and $\lambda>0$ is a parameter.

To summarize, the functional we proposed for image inpainting is

$$\begin{aligned}E(u)\ =&\ \frac{1}{2}\int_\Omega \alpha(f)|\Delta_{NL}u|^2\mathrm{d}x\\ &+\frac{\lambda}{2}\int_\Omega \chi_{\Omega-D}(x)(f-u)^2\mathrm{d}x.\end{aligned} \tag{8}$$

Besides, in the noiseless case, we constrain λ to be very large to ensure that the image is unchanged in the undamaged

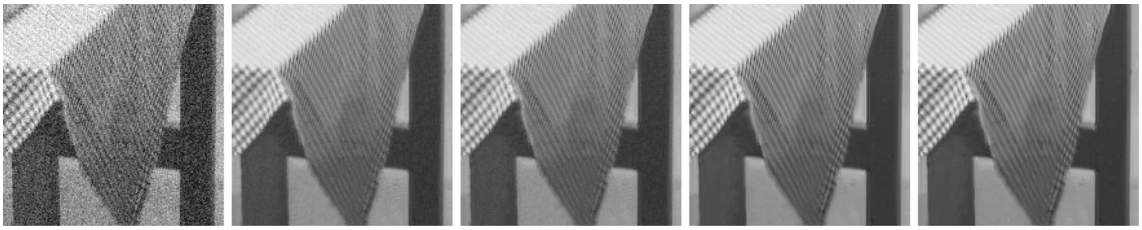

(a) Noisy **(b)** NLH **(c)** NLAH **(d)** NLBH **(e)** NLABH

Fig. 2 Comparison results between the NLH, NLAH, NLBH, and NLABH for image denoising

Table 1 Comparison of PSNR values of the different models

Model	PSNR
NLH (Fig. 2b)	29.584
NLAH (Fig. 2c)	29.591
NLBH (Fig. 2d)	30.800
NLABH (Fig. 2e)	30.804

region $\Omega - D$. The Euler–Lagrange equation associated with the functional (8), in a time-dependent fashion, is

$$\frac{\partial u}{\partial t} = -\Delta_{\mathrm{NL}}(\alpha(f)\Delta_{\mathrm{NL}}u) + \lambda\chi_{\Omega-D}(f-u). \tag{9}$$

We initialize $u(x,0) = f(x), x \in \Omega - D$, and $u(x,0)$ could be any value in the damaged region D. For simplicity, we set $u(x,0) = 255, x \in D$ in this paper.

For the image inpainting, we utilize the isotropic coefficient function $\alpha(f) = 1$. Because of the missing information, the adaptive coefficient function (4) may be not correct around the damaged region.

4 Mathematical Properties

In this section, we study the mathematical properties of the gradient descent scheme of $E(u)$, i.e.,

$$\begin{cases} \frac{\partial u}{\partial t} = -\Delta_{\mathrm{NL}}(\alpha(f)\Delta_{\mathrm{NL}}u) + \lambda K^*(f - Ku), \ (x,t) \in \Omega_T, \\ u(x,0) = f(x), \quad x \in \Omega, \end{cases} \tag{10}$$

where $f(x)$ is the initial condition, $\Omega_T = \Omega \times (0,T)$.

Throughout this section, we assume that $\Omega \subset \mathbb{R}^M$ ($M \geq 2$) is a bounded domain, $0 < \alpha_0 \leq \alpha(f) \leq \alpha_1 < 1$, $K : L^2(\Omega) \to L^2(\Omega)$ is a linear continuous operator and K^* denotes its adjoint operator. The nonlocal weight $w(x,y)$ is a nonnegative continuous symmetric function with compact support.

Theorem 1 *Let $f(x) \in L^2(\Omega)$. Problem (10) admits a unique solution $u \in C([0,T]; L^2(\Omega))$, such that*

$$\frac{\partial u}{\partial t} = -\Delta_{\mathrm{NL}}(\alpha(f)\Delta_{\mathrm{NL}}u) + \lambda K^*(f - Ku),$$

a.e. in Ω_T and $u(x,0) = f(x)$, a.e. in Ω.

Proof 1. Uniqueness. By the symmetry of $w(x,y)$, it is straightforward to verify that

$$\begin{aligned} &\int_\Omega \Delta_{\mathrm{NL}}u(x)\varphi(x)\mathrm{d}x \\ &\quad = -\frac{1}{2}\int_\Omega\int_\Omega w(x,y)\,(u(y)-u(x)) \\ &\qquad \times (\varphi(y)-\varphi(x))\,\mathrm{d}y\mathrm{d}x \\ &\quad = \int_\Omega u(x)\Delta_{\mathrm{NL}}\varphi(x)\mathrm{d}x, \end{aligned} \tag{11}$$

for any functions $u, \varphi \in L^2(\Omega)$.

Assume that u_1 and u_2 are two solutions of the problem (10) and $v = u_1 - u_2$. For a.e. $t \in [0,T]$, we have

$$\frac{\partial v}{\partial t} = -\Delta_{\mathrm{NL}}(\alpha(f)\Delta_{\mathrm{NL}}v) - \lambda K^*Kv.$$

Multiplying the above equality by v, integrating over Ω and utilizing (11), we get

$$\begin{aligned} \frac{1}{2}\int_\Omega \frac{\partial v^2}{\partial t}\mathrm{d}x = &-\int_\Omega \alpha(f)|\Delta_{\mathrm{NL}}v|^2\mathrm{d}x \\ &-\lambda\int_\Omega |Kv|^2\mathrm{d}x \leq 0. \end{aligned}$$

It follows from the initial condition $v(x,0) = 0$ that

$$\int_\Omega |u_1 - u_2|^2\mathrm{d}x = \int_\Omega |v|^2\mathrm{d}x \leq 0.$$

Consequently, $u_1(x,t) = u_2(x,t)$, a.e. in Ω_T.

2. Existence. For any $u \in C([0,t]; L^2(\Omega))$, we define an operator $\mathcal{L}$ as

$$\mathcal{L}u = f(x) - \int_0^t \Delta_{\mathrm{NL}}(\alpha(f)\Delta_{\mathrm{NL}}u)\mathrm{d}s + \lambda\int_0^t K^*(f-Ku)\mathrm{d}s.$$

Notice that

$$\begin{aligned}\int_\Omega |\mathcal{L}u - f(x)|^2\mathrm{d}x &\le 2\int_\Omega \left|\int_0^t \Delta_{\mathrm{NL}}(\alpha(f)\Delta_{\mathrm{NL}}u)ds\right|^2\mathrm{d}x \\ &\quad + 2\lambda^2\int_\Omega \left|\int_0^t K^*(f-Ku)ds\right|^2\mathrm{d}x \\ &\le Ct\max_{s\in[0,t]}\int_\Omega |u(x,s)|^2\mathrm{d}x \\ &\quad + Ct\int_\Omega |f|^2\mathrm{d}x.\end{aligned}$$

We select a small t_0 such that $\mathcal{L}$ maps from

$$X := \{u \in C([0,t_0]; L^2(\Omega)) : \|u\|_{C([0,t_0];L^2(\Omega))} \le M\}$$

into itself, where $M > 0$ is a constant.

For $u_1, u_2 \in X$, by direct calculation,

$$\begin{aligned}&\int_\Omega |\mathcal{L}u_1 - \mathcal{L}u_2|^2\mathrm{d}x \\ &\le Ct\max_{s\in[0,t]}\int_\Omega |u_1(x,s) - u_2(x,s)|^2\mathrm{d}x.\end{aligned}$$

We reselect t_0 such that $Ct_0 < 1$. Then $\mathcal{L}$ is a strict contraction in X, which means that problem (10) has a solution $u(x,t)$ for $t \in [0,t_0]$. By repeating, we can find a solution $u(x,t)$ for any $t \in [0,T]$.

Remark 1 Theorem 1 is also valid for the model of image inpainting Eq. (9) with the corresponding initial condition from the above proof process. Note, here the theorem is valid for the inpainting model (9) but not for the inpainting algorithm in Sect. 5.4 which is an iterative application of (9) with decreasing occlusion.

Next, we state that the solution of problem (10) preserves the mean value for image denoising.

Proposition 1 *If K is an identity operator, then*

$$\frac{1}{|\Omega|}\int_\Omega u(x,t)\mathrm{d}x = \frac{1}{|\Omega|}\int_\Omega f(x)\mathrm{d}x,$$

for any $t \ge 0$.

Proof Integrating the equation in (10) over Ω and recalling (11) to find

$$\begin{aligned}\int_\Omega \frac{\partial u}{\partial t}\mathrm{d}x &= -\int_\Omega \Delta_{\mathrm{NL}}(\alpha(f)\Delta_{\mathrm{NL}}u)\mathrm{d}x + \lambda\int_\Omega (f-u)\mathrm{d}x \\ &= \lambda\int_\Omega (f-u)\mathrm{d}x.\end{aligned}$$

Multiplying both sides by $e^{\lambda t}$, we have

$$\frac{\mathrm{d}}{\mathrm{d}t}\left(e^{\lambda t}\int_\Omega (u-f)\mathrm{d}x\right) = 0.$$

Then, the result follows from the initial condition $u(x,0) = f(x)$.

5 Numerical Implementation

Let u_i^n denotes the value of a pixel i in the image with time level n, where $i \in \Omega_d$ and $\Omega_d = \{1, 2, \cdots, N\}$ is the discretization of the image domain. The time step is τ, $t = n\tau$, $n = 0, 1, \cdots$. Let $w_{i,j}$ be the sparsely discrete version of $w = w(x,y) : \Omega \times \Omega \to \mathbb{R}$, and the construction details are given in Sect. 5.2 and 5.3. We use the neighbors set N_i defined by $N_i := \{j : w_{i,j} > 0\}$. Then, as in [18], the discretizations of the nonlocal gradient $\nabla_{\mathrm{NLd}}(u_i)$ and nonlocal Laplacian $\Delta_{\mathrm{NLd}}(u_i)$ are

$$\begin{aligned}\nabla_{\mathrm{NLd}}(u_i) &:= (u_j - u_i)\sqrt{w_{i,j}}, \quad j \in N_i, \\ \Delta_{\mathrm{NLd}}(u_i) &:= \sum_{j\in N_i}(u_j - u_i)w_{i,j},\end{aligned}$$

and the magnitude of the discrete nonlocal gradient is

$$|\nabla_{\mathrm{NLd}}(u_i)| := \sqrt{\sum_{j\in N_i}(u_j - u_i)^2 w_{i,j}}.$$

5.1 Finite Difference Schemes

To numerically solve the proposed models (6) and (8), we design two different finite difference schemes for their gradient descent schemes. Before that, we reformulate the equations (7) and (9) into same form,

$$\frac{\partial u}{\partial t} = -\Delta_{\mathrm{NL}}(\alpha(f)\Delta_{\mathrm{NL}}u) + \lambda(F_1 f - F_2 u),$$

where $F_1 = K^*$, $F_2 = K^*K$ for image deblurring and denoising and $F_1 = \chi_{\Omega-D}$, $F_2 = \chi_{\Omega-D}$ for image inpainting.

We first give the finite difference explicit scheme, as follows:

$$\begin{aligned}\frac{u_i^{n+1} - u_i^n}{\tau} &= -\Delta_{\mathrm{NLd}}(\alpha(f_i)\Delta_{\mathrm{NLd}}(u_i^n)) \\ &\quad + \lambda(F_1 f_i - F_2 u_i^n). \qquad (12)\end{aligned}$$

For the semi-implicit scheme, we first expand the proposed fourth-order regularizer as

$$-\Delta_{\mathrm{NL}}(\alpha(f)\Delta_{\mathrm{NL}}u) = -\int_{\Omega}(\alpha(f)(y)\Delta_{\mathrm{NL}}u(y) - \alpha(f)(x)\Delta_{\mathrm{NL}}u(x))\,w(x,y)\mathrm{d}y,$$

where $\Delta_{\mathrm{NL}}u(y)=\int_{\Omega}(u(z)-u(y))w(y,z)\mathrm{d}z$ and $\Delta_{\mathrm{NL}}u(x)=\int_{\Omega}(u(z')-u(x))w(x,z')\mathrm{d}z'$. Thus, the regularization term is equal to

$$\begin{aligned}&-\int_{\Omega}\alpha(f)(y)\cdot\int_{\Omega}(u(z)-u(y))w(y,z)\mathrm{d}z\cdot w(x,y)\mathrm{d}y\\&+\int_{\Omega}\alpha(f)(x)\cdot\int_{\Omega}u(z')w(x,z')\mathrm{d}z'\cdot w(x,y)\mathrm{d}y\\&-\alpha(f)(x)\cdot u(x)\int_{\Omega}\int_{\Omega}w(x,z')\mathrm{d}z'\cdot w(x,y)\mathrm{d}y.\end{aligned}$$

Notice, the u in the last term of the above formula is independent of the integration, and we discretize it in the $n+1$ level. Therefore, the semi-implicit scheme is

$$\begin{aligned}&\frac{u_i^{n+1}-u_i^n}{\tau}+\alpha(f_i)\cdot u_i^{n+1}\sum_{j\in N_i}\left(w_{i,j}\sum_{k'\in N_i}w_{i,k'}\right)\\&=-\sum_{j\in N_i}\alpha(f_j)\Delta_{\mathrm{NLd}}(u_j^n)\cdot w_{i,j}\\&\quad+\alpha(f_i)\sum_{j\in N_i}\sum_{k'\in N_i}(u_{k'}^n\cdot w_{i,j}\cdot w_{i,k'})+\lambda(F_1f_i-F_2u_i^n).\end{aligned}\tag{13}$$

For the explicit scheme (12) and semi-implicit scheme (13), u_i^{n+1} can be expressed explicitly.

5.2 Construction of the Weight Matrix

We construct the weight matrix $w=(w_{i,j})_{N\times N}$ of the discrete image $u_i, i\in\Omega_d$. For each pixel, compare the distances to all the patches in the search window. Denote the patch centered at the pixel i as P_i, and the size is $lp\times lp$. And, extend the image with periodic boundary condition to get all of the patches. Besides, denote the set of the pixels in the search window as $S(i)$, and the size of the search window is $lw\times lw$.

First, we need to calculate the weighted Euclidean distance. For the image deblurring and denoising, the distance is $d(u)_{i,j}=\|P_i-P_j\|_{2,a}^2, j\in S(i)$, where $a>0$ is the standard deviation of the Gaussian kernel. For image inpainting, with the un-recovered region $R\subset D_d$ (D_d is the discretization of the damaged region D), the patch distance for each pixel i is

$$d^R(u)_{i,j}=\sum_{i+k\in P_i^v,\ j+k\in P_j^v}(g_a)_{c+k}\cdot\|u_{i+k}-u_{j+k}\|^2,$$

where $P_i^v=P_i^{idx}\cap(\Omega_d-R)$, $P_j^v=P_j^{idx}\cap(\Omega_d-R)$, P_i^{idx} and P_j^{idx} are the sets of pixels (location) of patches P_i and P_j, respectively, and g_a is the Gaussian kernel (c is the central location).

We construct the neighbors set N_i by taking the m most similar and the four nearest neighbors of the pixel i, where $m\geq 0$ is a parameter. In this paper, we set m to the half-length of the search window, that is, $m=\lfloor lw/2\rfloor$. Especially, setting the coordinate of pixel i to (i_x,i_y), the four nearest neighbors are (i_x-1,i_y), (i_x+1,i_y), (i_x,i_y-1), and (i_x,i_y+1). The nonlocal weights are defined as follows:

$$w_{i,j}=\begin{cases}\mathrm{e}^{-\frac{d(u)_{i,j}}{2h^2}}, & i\in\Omega_d,\ j\in N_i,\\ 0, & \text{others},\end{cases}\tag{14}$$

for image deblurring and denoising, and

$$w_{i,j}=\begin{cases}\mathrm{e}^{-\frac{d^R(u)_{i,j}}{2h^2}}, & i\in\Omega_d,\ j\in N_i,\ P_i^v\neq\emptyset,\\ & P_j^v\neq\emptyset,\ (P_i^v-\{i\})\cap(P_j^v-\{j\})\neq\emptyset,\\ 0, & \text{others}.\end{cases}\tag{15}$$

for image inpainting, where $h>0$ is a modulation parameter. It is worth noting that set u as the observed f in (14) corresponding to the model (7), and for inpainting the choice of u in (15) depends on the inpainting algorithm(Sect. 5.4). Especially, for image inpainting, after obtaining the normal weight function $w_{i,j}$, we utilize the weight matrix normalization (18) to get w', and the details are presented in Sect. 5.3. Besides, to confirm the symmetry constraint, for image deblurring and denoising, set

$$w_{i,j}=\max(w_{i,j},w_{j,i}),\quad\forall i,j\in\Omega_d,\tag{16}$$

and for image inpainting, set

$$w'_{i,j}=\max(w'_{i,j},w'_{j,i}),\quad\forall i,j\in\Omega_d.\tag{17}$$

Correspondingly, we need to update the neighbors set N_i for $i\in\Omega_d$.

For the image deblurring and denoising, the weight matrix w is calculated by the degradation image f without updating during the evolution. The reason is that if we update the weight matrix during the restoration process, it is not easy to choose when to update, and also the parameters for the weight matrix calculation are not easy to tune for better restoration results than the case without updating. For image inpainting, the weight matrix w' has to be updated to recover the whole image. The detailed algorithm is presented in Sect. 5.4.

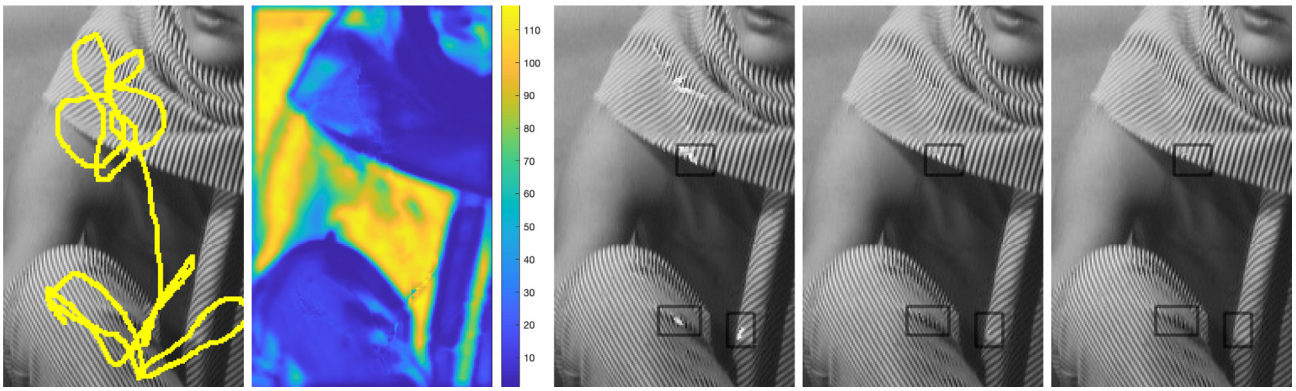

(a) Damaged **(b)** $w \times \mathbf{1}$ **(c)** w, 1000th **(d)** w, 10000th **(e)** w', 50th

Fig. 3 Inpainting result by the proposed nonlocal biharmonic model with original method of w and normalized w' (finite difference scheme, semi-implicit one). **a** Damaged image. **b** $w \times \mathbf{1}$, $\mathbf{1}_{N\times 1}$ is the one vector, parameters of w: patch size $lp = 7$, search window $lw = 11$. **c** Inpainted with w in 1000th iteration. **d** Inpainted with w in 10000th iteration. **e** Inpainted with normalized w' in 50th iteration

5.3 Weight Matrix Normalization

For image inpainting, if there are few similar patches for the damaged patch, its corresponding sum of weights is very small and very large iterations are needed to recover the pixel, which means different inpainting rates for different pixels. Figure 3b shows the map of $w \times \mathbf{1}$ which is the sum of each row of w. If we employ the weight matrix w (Eq. 15), the relative weight of the effective similar block would be very small for these dark blue pixels in Fig. 3b. As shown in Fig. 3c, d, it needs very large iterations to inpaint in the gray box regions.

To solve this, we develop a weight matrix normalization method to obtain the normalized weights w' for the inpainting process. In detail, for each row of weight matrix w,

$$w'_{i,j} = \begin{cases} 0, & j = i, \\ \dfrac{w_{i,j}}{\sum\limits_{k,k\neq i} w_{i,k}}, & j \neq i, \end{cases} \tag{18}$$

for $\forall i, j \in \Omega_d$. In this case, the sum of all weights of each row is 1. We do not employ the weight for the block itself. For image inpainting, the main point is to find similar blocks and inpaint the damaged area according to these similar blocks and the corresponding similarity values. Thus, the weight of itself is not necessary. And, averaging every row makes the similarity values of the same magnitude. At the same time, if we apply the finite difference scheme, the largest time step confirming stability can be larger. The inpainting result with normalized weight w' is shown in Fig. 3e. It only need 50 iterations which is much less than the one using the original weight w.

5.4 Algorithm of Inpainting

The inpainting procedure by the proposed model produces the discrete un-recovered regions D_d^k, $k = 1, 2, \cdots$, with $D_d^0 = D_d$ and $D_d^0 \supset D_d^1 \supset D_d^2 \supset \cdots$. Similar to [24], we update the weight matrix w' after the current inpainting process reaches a steady state. The inpainting procedure is as follows:

(1) Compute weights matrix w' by Eqs. (15), (18), and (17) with damaged region Ω_d^0 and initial image u^0.
(2) Iterate $k = 1, 2, \cdots$ to obtain the steady state of the proposed inpainting method, the inpainted image u^k and un-recovered region Ω_d^k. Update the weight matrix w' with Ω_d^k and u^k until $D^k = \emptyset$.

The above inpainting algorithm is an iterative application of the model (9) with decreasing occlusions. Usually, there is no noise in the damaged image f, and we take a hard constraint to ensure that $u^k = f$ in the undamaged region $\Omega_d - D_d$ and only update the image in D_d for each iteration of the scheme (12) or (13).

6 Experiments

In order to quantify the restoration effect, for the original clean image u_{O} and its restored image u, the restoration performance is measured in terms of peak signal-to-noise ratio (PSNR)[14],

$$\mathrm{PSNR} = 10\log_{10}\frac{M_1 N_1 |\max u_{\mathrm{O}} - \min u_{\mathrm{O}}|^2}{\|u - u_{\mathrm{O}}\|_{L^2}^2}\mathrm{dB},$$

and mean absolute deviation error (MAE),

$$\text{MAE} = \frac{\|u - u_0\|_{L^1}}{M_1 N_1},$$

where $M_1 \times N_1$ is the size of the image. Besides, we also use the structural similarity (SSIM) [47]. All of the image restoration results by the proposed model are obtained using the semi-implicit scheme (13). And all of the other parameters in the methods are tuned to reach maximal PSNR values.

6.1 Comparison Between the Two Schemes

We compare the difference between the explicit scheme (12) and semi-implicit scheme (13), taking the denoising problem (K is the identity) as an example. The comparison results are shown in Fig. 4. All of the parameters of the two schemes are same except the time step τ. The test noisy image is Fig. 4a, and we set $\lambda = 10$ for the proposed model (6). The denoising results are almost the same by different schemes and time step τ. From the simulation, the maximal time step τ of the explicit scheme (12) is 0.0005, but the time step of the semi-implicit scheme could be any large value ($\lambda = 10$). We show the energy changes over time and over iterations in Fig. 4e, f, respectively. As the evolution over time, the energy value decreases until it stabilizes by each scheme. And from Fig. 4f, we only need small number of iterations to reach the steady state by the semi-implicit scheme (13).

However, the time step size that the semi-implicit scheme (13) allows may be not arbitrary if the parameter λ is larger (or with other weight matrix parameters), such as that if we set $\lambda = 20$, the maximal τ is 0.0004 for the the explicit scheme (12) and 0.3 for the semi-implicit scheme (13).

All of these indicate that the semi-implicit scheme (13) has better stability and allows a larger time step size than the explicit scheme (12). Because these two schemes evolute totally same numerical results, we only employ the semi-implicit scheme (13) for the following experiments.

6.2 Image Deblurring and Denoising

We first apply our proposed model to image denoising, and thus, this is when the blur kernel K is the identity. To study the performance of our method, we compare the proposed model with the local fourth-order diffusion model AFD [20], NLTV, and BM3D [11], and results are shown in Table 2 and Figs. 5 and 6. About the choice of parameter λ for image denoising, for both the NLTV and proposed model, we set $\lambda = 0$ and stop the iteration when achieve best PSNR values to clearly show the smoothing and edge preservation abilities of the regularizer. Besides, restoration results by two adaptive coefficients Eqs. (4) and (5) are similar, and the nonlocal version is a little bit better. Thus, we employ the nonlocal gradient-based adaptive coefficient function (5) in the following experiments.

For the synthetic image Fig. 5b containing smooth surfaces and sharp edges, the local fourth-order model AFD [20] can restore the smooth areas while preserving edges very well. The BM3D [11] method generates artifacts around edges. Compared with NLTV, the proposed model can restore homogeneous regions smoothly, and the lines restored more sharp and clean. For the real image *Lena*, the proposed model can better preserve both sharp and blunt lines in the image. Figure 6 shows denoising results of the texture image (*Barbara*). Because the local method does not work well in textured regions, we only show the results of the BM3D [11], NLTV, and proposed model. The denoised images by the proposed model are smoother; simultaneously, texture and edges are preserved. Moreover, the homogeneous areas and lines recovered by the NLTV are not smooth enough. From Fig. 6, compared with NLTV, the proposed model can restore these blunt texture at the upper part of the tablecloth. The BM3D [11] method can preserve textures very well, but artificial effects show again around the arm. The denoising results of our proposed model are more natural visually, especially in homogeneous regions. All of these verify the effectiveness of the proposed model for image denoising.

And then, we compare the IVM [50], MSPB [40],[1] NLIP [34], [2] and proposed model for image deblurring and denoising. The IVM [50] is a variational model based on local second-order variation and splitting technique. The MSPB [40] extends the expected patch log likelihood by considering a multi-scale prior. The NLIP [34] is a NLTV-based image restoration method which utilizes the Tikhonov regularization as the preprocessor. For the proposed model, employ the nonlocal gradient-based coefficient (5), stop the iteration of the semi-implicit scheme when reaching the energy stable status, and tune the regularization parameter λ to achieve the best performance. Also, the choices of parameter λ for the NLIP [34] and proposed model are listed in Table 3. Simulation experiment results are shown in Fig. 7. The corresponding comparison of PSNR, MAE, and SSIM is listed in Table 3.

From the *synthetic*, compared with the NLIP [34] model, the proposed model has a good performance at restoring the curved surface. The NLIP [34] model restores sharp jumps better. Moreover, from the natural image *Lena* and the other two texture images, the restored images obtained using the proposed model are cleaner than the ones obtained by the NLIP [34], and the lines restored by the proposed model are more fluent without serrated edges. The local derivative-based model IVM [50] restore the rough structure, but can not restore flowing lines and fine texture. The patch-based method MSPB [40] smooth the noise very well, but can not restore sharp edges and textures. The comparison of the

[1] https://github.com/ngcthuong/Image-Denoising-Benchmark.

[2] https://math.sjtu.edu.cn/faculty/xqzhang/NLIP_v1.zip.

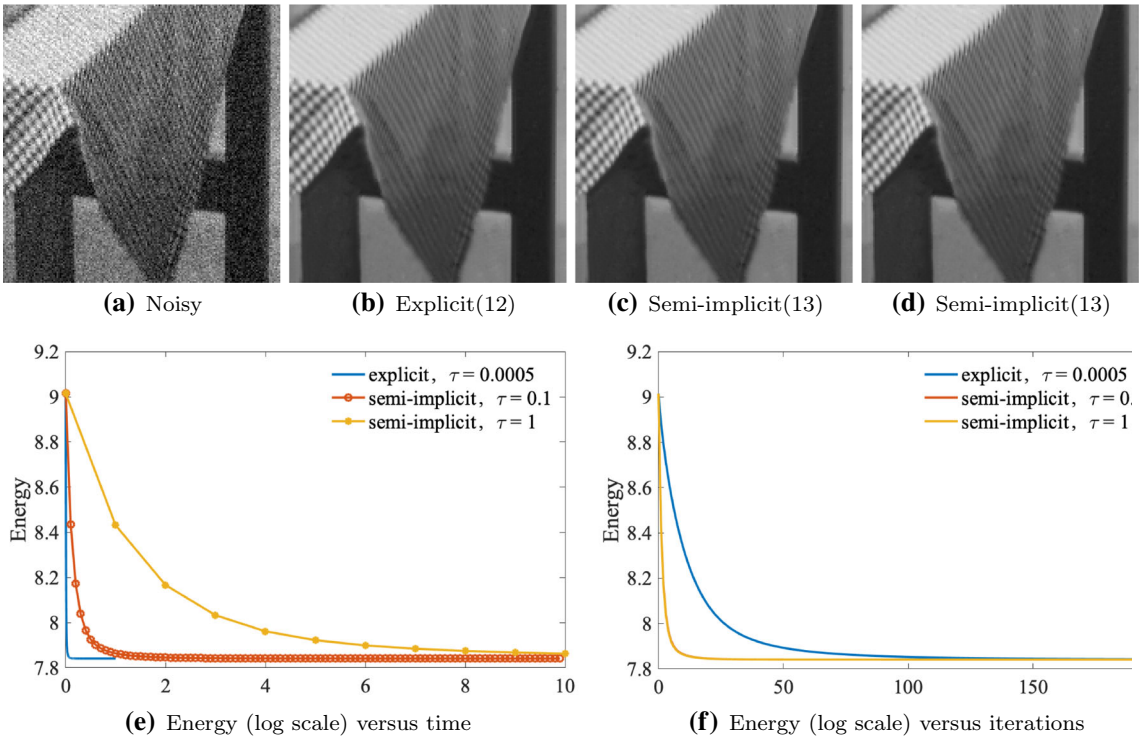

Fig. 4 Comparison of the explicit scheme and semi-implicit scheme with parameter $\lambda = 10, lp = 11, lw = 31$, and $h = 70.71$. **a** Test noisy image. **b** Denoising result by the explicit scheme with $\tau = 0.0005$ (PSNR 28.672). **c** Denoising result by the semi-implicit scheme with $\tau = 0.1$ (PSNR 28.672). **d** Denoising result by the semi-implicit scheme with $\tau = 1$ (PSNR 28.672). **e** Energy versus time t of different schemes with common logarithm scale on energy. **f** Energy versus iterations of different schemes with common logarithm scale on energy

Table 2 Comparison of PSNR, MAE, and SSIM of the different models with Gaussian noise, and noise level $\sigma_n = 10, 20, 30$

σ_n	PSNR			MAE			SSIM		
	10	20	30	10	20	30	10	20	30
Synthetic									
AFD [20]	40.156	36.103	34.096	1.546	2.501	3.355	0.484	0.455	0.437
BM3D [11]	**43.110**	**38.411**	**35.494**	0.997	1.850	2.749	0.498	0.456	0.415
NLTV	42.074	36.921	35.042	0.964	1.906	2.419	**0.765**	**0.481**	**0.450**
Proposed	42.775	38.224	35.323	**0.824**	**1.531**	**2.273**	0.752	0.470	0.439
Lena									
AFD [20]	32.892	29.542	27.769	4.054	5.874	7.183	0.747	0.649	0.586
BM3D [11]	**35.456**	**31.735**	**29.623**	**3.067**	**4.572**	**5.792**	**0.775**	**0.683**	**0.606**
NLTV	34.562	30.820	28.802	3.458	5.151	6.455	0.743	0.630	0.559
Proposed	34.992	31.464	29.348	3.250	4.735	6.045	0.768	0.663	0.583
Barbara									
BM3D [11]	**35.410**	**32.116**	**30.013**	**3.245**	**4.607**	**5.870**	0.752	**0.669**	**0.591**
NLTV	34.371	30.377	28.575	3.633	5.648	6.863	0.724	0.601	0.521
Proposed	35.046	31.729	29.619	3.359	4.803	6.164	**0.757**	0.661	0.572

Bold values indicate the best results in the comparison experiment

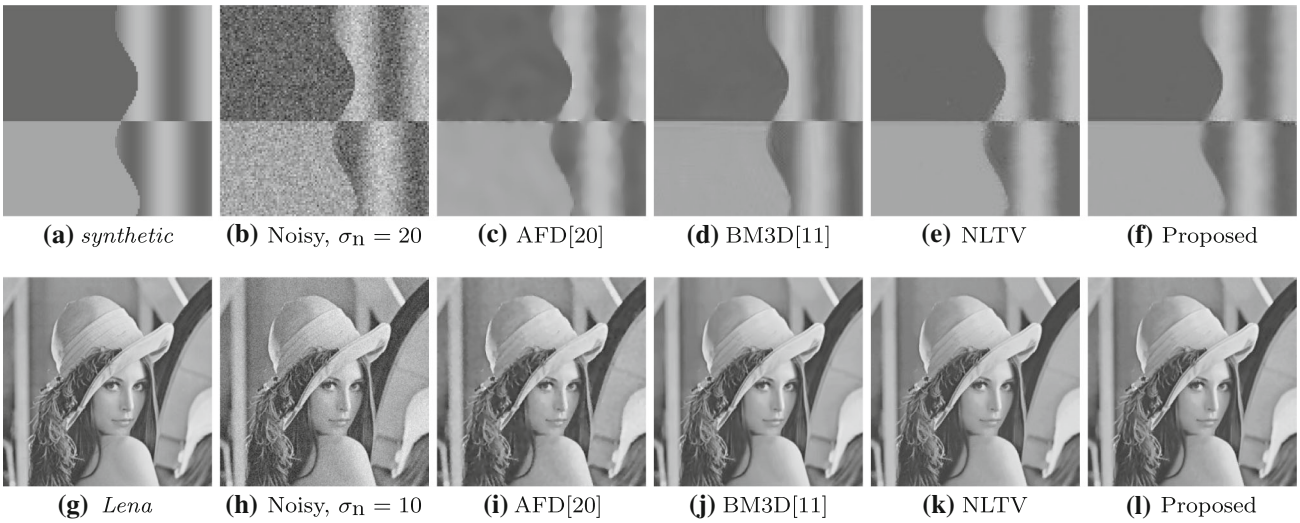

Fig. 5 Denoising results of *synthetic* and *Lena*. The noise level of the noisy *synthetic* and *Lena* is 20 and 10, respectively. Weight matrix parameters of the proposed model are $lp = 11, lw = 51, h = 20$ for *synthetic* and $lp = 9, lw = 51, h = 20$ for *Lena*

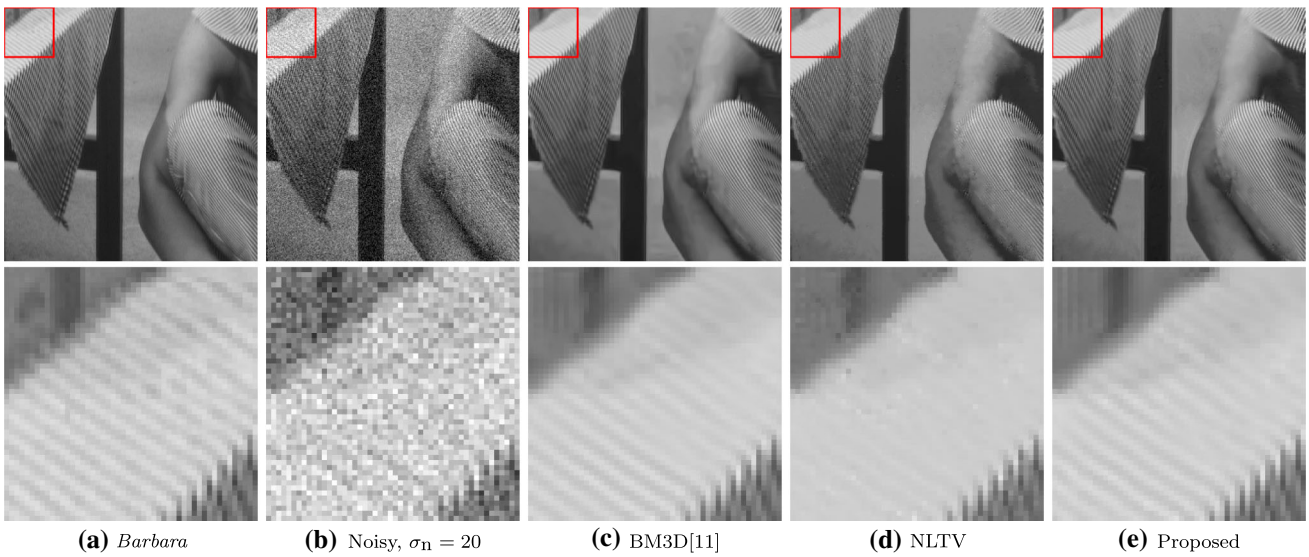

Fig. 6 Denoising results of *Barbara* with enlarged part of corresponding red boxes. The noise level of the noisy *Barbara* is 20. Weight matrix parameters of the proposed model are $lp = 13, lw = 41, h = 25$ (Color figure online)

image quality measurement index in Table 3 also verifies the effectiveness of the proposed method.

6.3 Image Inpainting

In this subsection, we compare the inpainting performance of our proposed model with the NLTV, NLH, local biharmonic model (BH), and nonlocal patch-based method (NLPB) [38]. [3] Here, the BH model means utilizing the purely biharmonic regularization. We employ the semi-implicit scheme for image inpainting. And all of the parameters are tuned to confirm best performances for the NLPB [38], BH, NLTV, NLH, and proposed model. Note the inpainting framework in Sect. 5.4 are also applied to the NLTV and NLH. The PSNRs of inpainting results are shown in Table 4. As shown in Figs. 8, 9, 10, 11 and 12, we utilize the proposed regularizers to recover images with rectangle, scratch, and words missing regions. From Table 3, the NLTV method does not perform as well as the NLH model, so for simplicity, we only show its results for Figs. 8 and 9.

In Figs. 8 and 9, we show the inpainting results of the comparison methods and the process of the proposed inpainting with a rectangle missing region. From Table 4, the PSNR values of our proposed model are the highest. Visually, the proposed model performs better than the other methods in the texture, edge and homogeneous regions inpainting. The

[3] https://www.ipol.im/pub/art/2017/189/Inpainting_ipol_code.tar.gz.

Table 3 Comparison of PSNR, MAE, and SSIM of the different models with different blur and noise

	Gaussian blur σ_b	Gaussian noise σ_n	Model	λ	PSNR	MAE	SSIM
Synthetic	2	7	IVM [50]	–	34.500	3.951	0.974
			MSPB [40]	–	34.050	4.014	**0.979**
			NLIP [34]	20	**34.502**	**3.869**	0.978
			Proposed	50	33.545	4.116	0.971
Lena	2	7	IVM [50]	–	28.506	6.543	0.858
			MSPB [40]	–	28.249	6.611	0.845
			NLIP [34]	20	28.341	6.586	0.853
			Proposed	2000	**28.562**	**6.417**	**0.863**
Barbara1	1	7	IVM [50]	–	23.755	12.572	0.626
			MSPB [40]	–	21.426	16.347	0.369
			NLIP [34]	100	23.180	13.510	0.575
			Proposed	10,000	**23.797**	**12.181**	**0.631**
Barbara2	1	10	IVM [50]	–	27.398	8.155	0.805
			MSPB [40]	–	26.152	9.250	0.664
			NLIP [34]	60	27.296	8.327	0.812
			Proposed	1000	**27.502**	**7.918**	**0.830**

Bold values indicate the best results in the comparison experiment

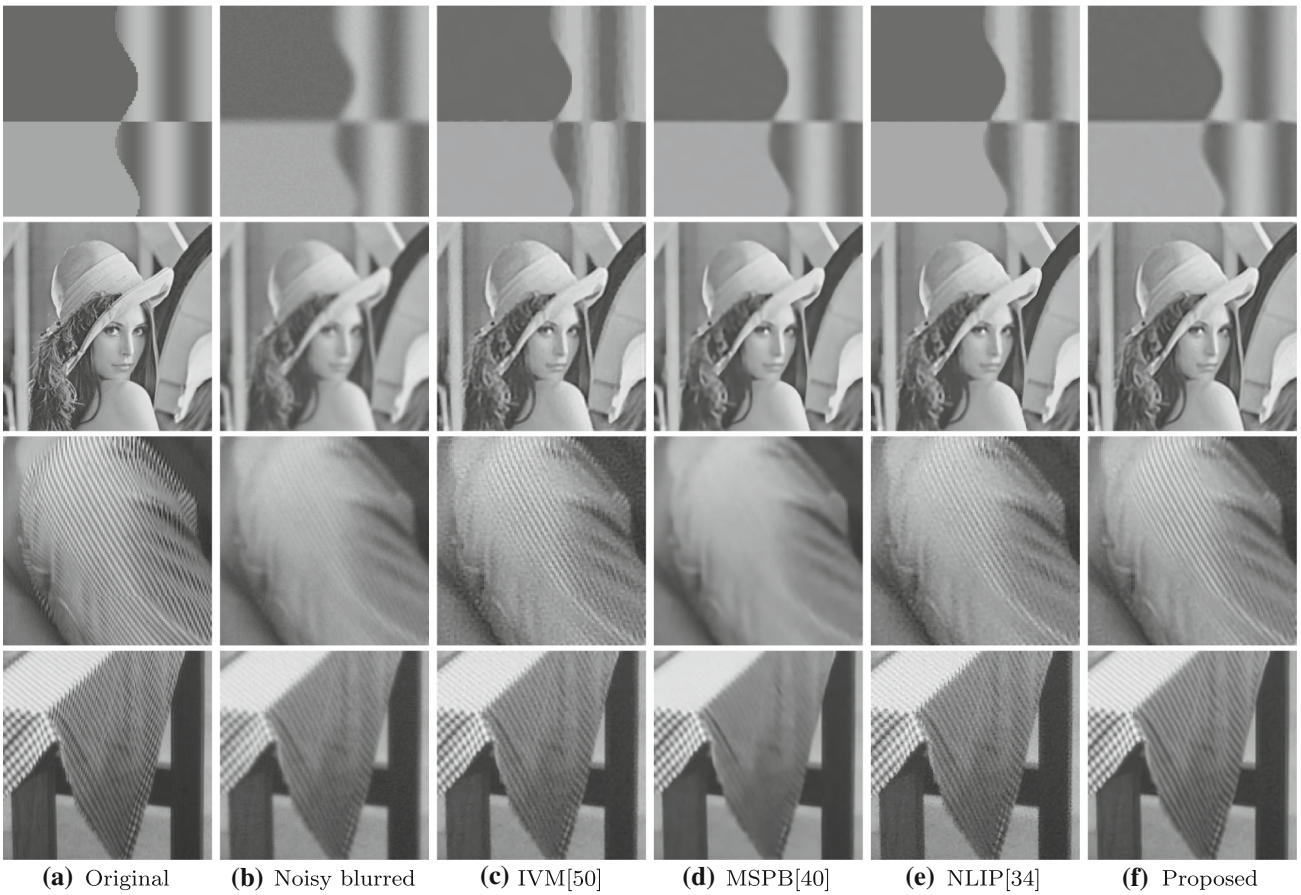

Fig. 7 Deblurring and denoising results of *synthetic*, *Lena*, *Barbara1*, and *Barbara2* utilizing the IVM [50], MSPB [40], NLIP [34] and proposed model. From top to bottom: *synthetic*, $\sigma_b = 2$, $\sigma_n = 7$; *Lena*, $\sigma_b = 2$, $\sigma_n = 7$; *Barbara1*, $\sigma_b = 1$, $\sigma_n = 7$; *Barbara2*, $\sigma_b = 1$, $\sigma_n = 10$. Weight matrix parameters of the proposed model are $lp = 3$, $lw = 11$, $h = 10$ for *synthetic*, $lp = 9$, $lw = 25$, $h = 10$ for *Lena*, $lp = 9$, $lw = 37$, $h = 10$ for *Barbara1*, and $lp = 9$, $lw = 37$, $h = 10$ for *Barbara2*.

Table 4 Comparision of PSNR of the different methods for inpainting

	NLPB [38]	BH	NLTV	NLH	Proposed
Figure 8	37.230	34.833	36.115	37.513	**38.676**
Figure 9	35.204	33.2433	37.955	38.079	**38.608**
Figure 10 first row	32.667	35.337	34.482	35.159	**35.523**
Figure 10 second row	30.662	31.015	30.146	30.945	**31.087**
Figure 11 first row	39.355	39.157	38.582	39.219	**39.945**
Figure 11 second row	32.706	**33.440**	31.169	32.032	32.960
Figure 12 first row	20.641	21.266	20.628	21.101	**21.522**
Figure 12 second row	**27.891**	23.338	21.197	21.458	22.108
Figure 12 third row	**24.760**	24.097	23.043	24.047	24.164

Bold values indicate the best results in the comparison experiment

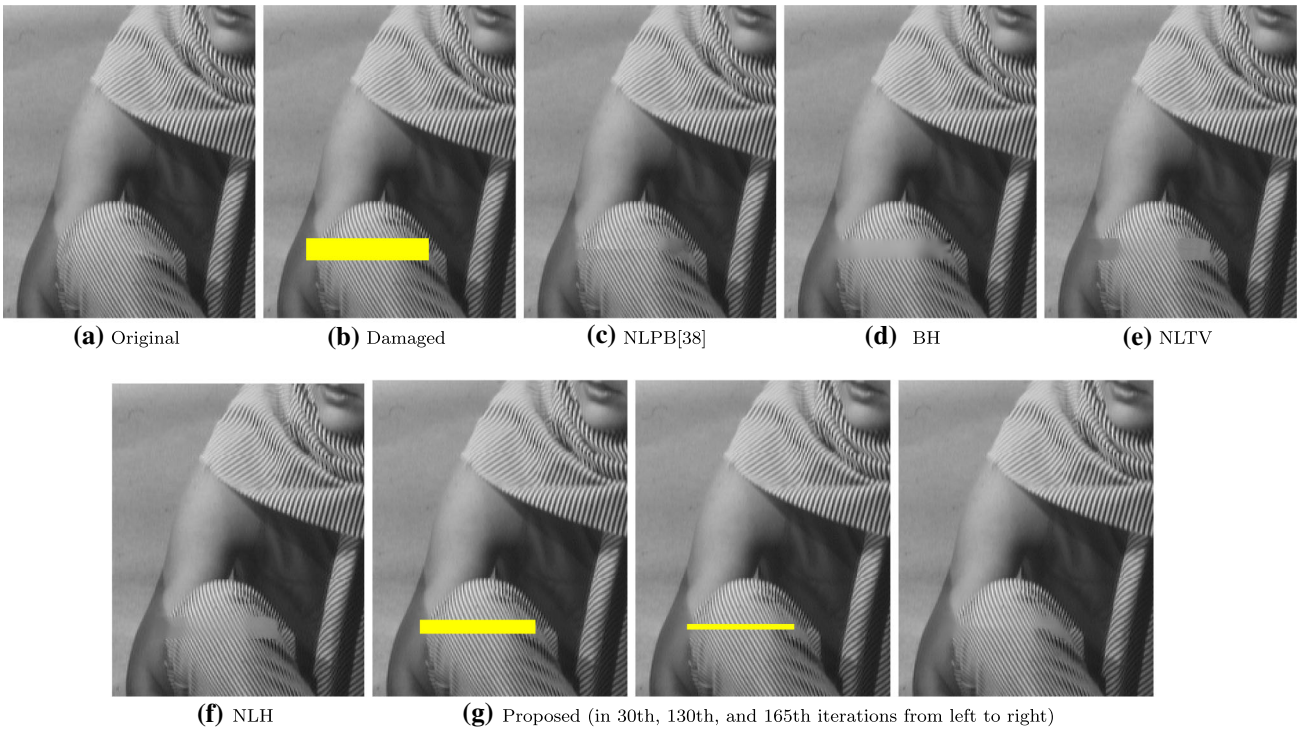

(a) Original **(b)** Damaged **(c)** NLPB[38] **(d)** BH **(e)** NLTV

(f) NLH **(g)** Proposed (in 30th, 130th, and 165th iterations from left to right)

Fig. 8 Inpainting results of image with 183×16 missing part. Weight matrix parameters of the proposed model are $lp = 7, lw = 11, h = 8$.

patch-based method NLPB [38] generates shocks and undesired artifacts near the medial axis of the occlusion as shown in Fig. 9c. On the other hand, the NLPB [38] can produce a consistent and plausible continuation of the texture as shown in Fig. 9b. The local biharmonic model BH can not recover lines and results in blur. The inpainting results of the proposed model are more consistent and contain richer details, especially in the areas with weak texture and edge.

We give a group of experiments with scratch damage in Fig. 10. These visually seem to produce very similar results, but from the PSNR values in Table 4 our proposed model performs better than the other methods. Word damage inpainting results are shown in Fig. 11. The proposed method can recover images with more flowing lines and smooth regions from the hair and the bridge of the nose of the girl. The local method BH can inpaint homogeneous parts very well, but it can not restore lines clearly. The NLPB [38] method would destroy fluent lines, and it can not maintain consistency.

At last, we illustrate the effectiveness of our method for texture image inpainting (Fig. 12). We choose three texture images and destroy them with three different damage regions, respectively. For the NLPB [38] method, it has the advantage of recovering images with rich repeated structures. The recovered images by the proposed method are more natural than ones by the BH and NLH methods. We still can see the shape of the damaged region in the recovered image by the BH and NLH methods, especially the last row of Fig. 12.

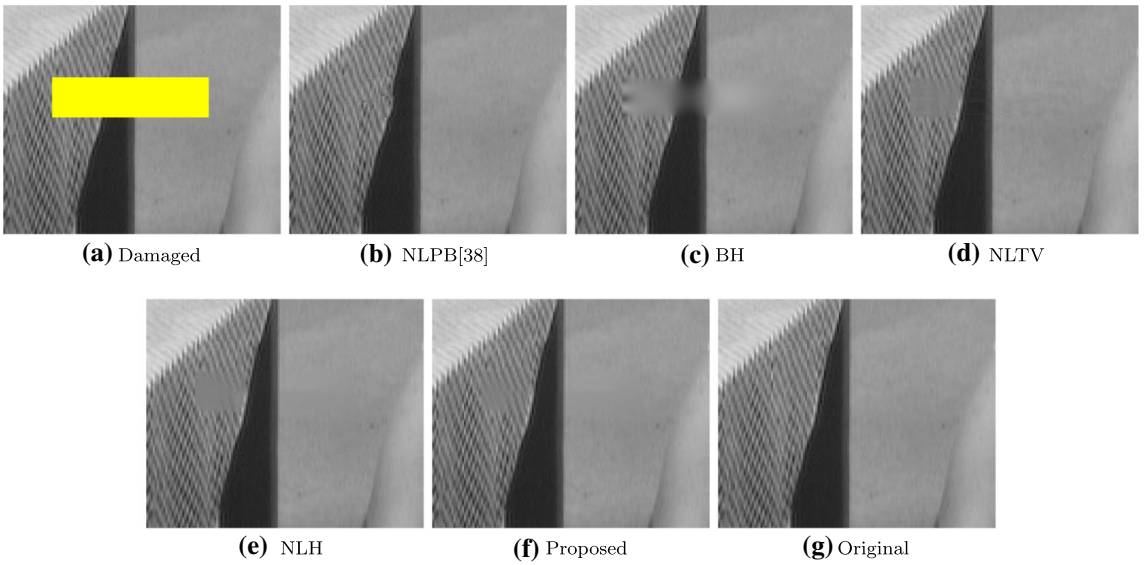

Fig. 9 Inpainting results of image with 19×74 missing part. Weight matrix parameters of the proposed model are $lp = 7, lw = 11, h = 8$.

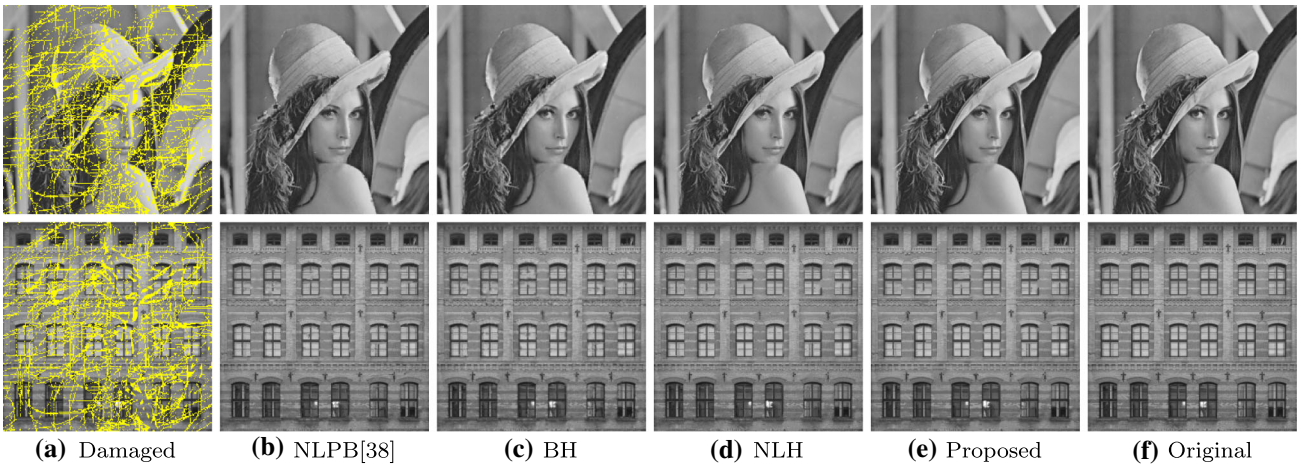

Fig. 10 Inpainting results of images with scratch damage. Weight matrix parameters of the proposed model are $lp = 7, lw = 11, h = 8$ for the first row and $lp = 5, lw = 11, h = 7$ for the second row

(a) Damaged **(b)** NLPB[38] **(c)** BH **(d)** NLH **(e)** Proposed **(f)** Original

Fig. 11 Inpainting results of image with word damages. Weight matrix parameters of the proposed model are $lp = 7, lw = 11, h = 8$ for the first row and $lp = 5, lw = 11, h = 8$ for the second row

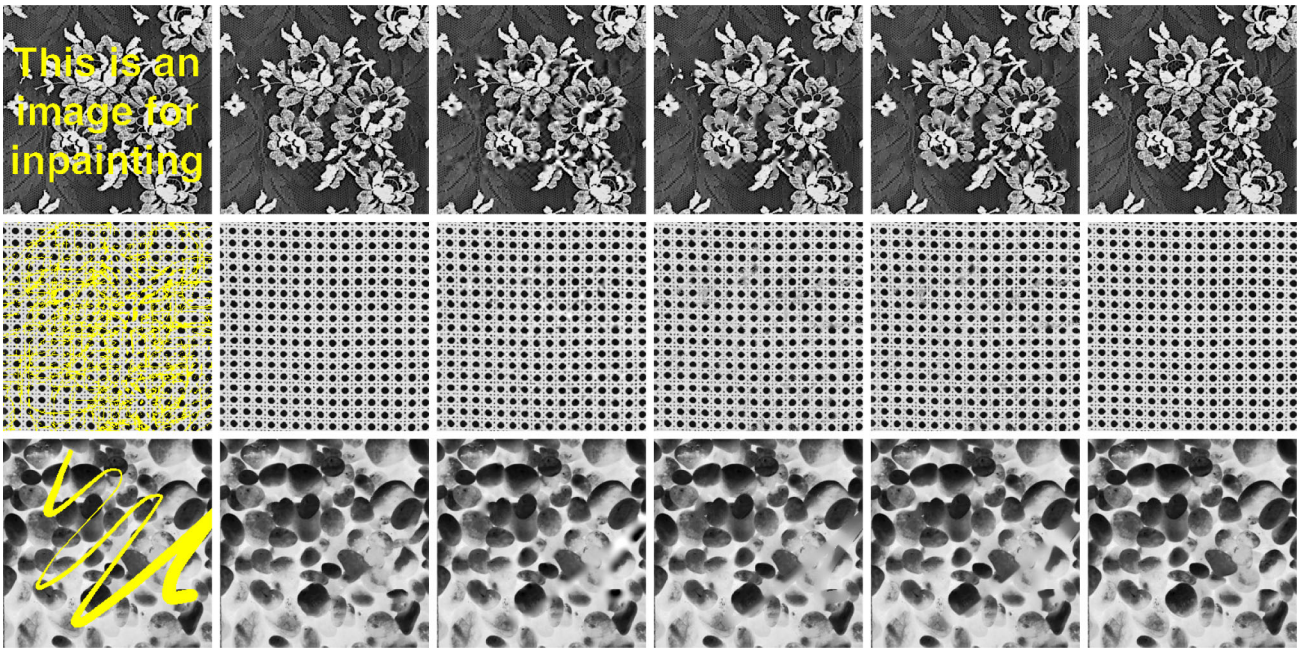

(a) Damaged **(b)** NLPB[38] **(c)** BH **(d)** NLH **(e)** Proposed **(f)** Original

Fig. 12 Inpainting results of texture images with three different damages. Weight matrix parameters of the proposed model are $lp = 5, lw = 11, h = 25$ for the first row, $lp = 7, lw = 11, h = 28$ for the second row, and $lp = 5, lw = 11, h = 30$ for the third row

7 Conclusion

We have proposed in this paper an anisotropic nonlocal fourth-order biharmonic regularizer for image restoration, and we have shown through experiments and deduction that the nonlocal biharmonic model is better than the nonlocal harmonic model at slope preservation. We have applied the proposed regularizer to image deblurring and denoising and image inpainting. A weight matrix normalization has been proposed to speed up the image inpainting process. The uniqueness and existence of the solution and the mathematical property of the proposed model have been proved. We have discretized the model using finite difference schemes that are stable in practice. We have presented numerous experimental results on synthetic and real images that show the advantages of the proposed model, by comparison with local fourth-order models, nonlocal second-order models, and other state-of-the-art methods.

Acknowledgements This work was partially supported by the NSF grant 2012868, the National Natural Science Foundation of China (12001509, 11871133, U21B2075, 11971131, 61873071, 51476047), the Natural Science Foundation of Zhejiang Province (LQ21A010010),

Natural Sciences Foundation of Heilongjiang Province (ZD2022A001), the Fundamental Research Funds for the Central Universities (HIT.NSRIF202202), and China Society of Industrial and Applied Mathematics Young Women Applied Mathematics Support Research Project.

Declarations

Conflict of interest The authors declare that they have no conflict of interest.

References

1. Ambrosio, L., Tortorelli, V.M.: On the approximation of free discontinuity problems. pp. 105–123 (1992)
2. Atlas, A., Bendahmane, M., Karami, F., Meskine, D., Oubbih, O.: A nonlinear fractional reaction-diffusion system applied to image denoising and decomposition. Discrete Continuous Dyn. Syst. B **26**(9), 4963 (2021)
3. Bertalmio, M., Bertozzi, A.L., Sapiro, G.: Navier-Stokes, fluid dynamics, and image and video inpainting. In: Proceedings of the 2001 IEEE Computer society conference on computer vision and pattern recognition. CVPR 2001, **1**, I–I (2001) IEEE
4. Bertalmio, M., Sapiro, G., Caselles, V., Ballester, C.: Image inpainting. In: Proceedings of the 27th annual conference on Computer graphics and interactive techniques, pp. 417–424 (2000)
5. Bertozzi, A.L., Greer, J.B.: Low-curvature image simplifiers: global regularity of smooth solutions and laplacian limiting schemes. Commun. Pure Appl. Math. J. Issued Courant Inst. Math. Sci. **57**(6), 764–790 (2004)
6. Buades, A., Coll, B., Morel, J.M.: A non-local algorithm for image denoising. In: 2005 IEEE Computer Society conference on computer vision and pattern recognition (CVPR'05), **2**, 60–65 (2005) IEEE
7. Chambolle, A., Lions, P.L.: Image recovery via total variation minimization and related problems. Numer. Math. **76**(2), 167–188 (1997)
8. Chan, R.H., Chen, K.: A multilevel algorithm for simultaneously denoising and deblurring images. SIAM J. Sci. Comput. **32**(2), 1043–1063 (2010)
9. Chan, T., Marquina, A., Mulet, P.: High-order total variation-based image restoration. SIAM J. Sci. Comput. **22**(2), 503–516 (2000)
10. Chen, D., Sun, S., Zhang, C., Chen, Y., Xue, D.: Fractional-order tv-l 2 model for image denoising. Cent. Eur. J. Phys. **11**(10), 1414–1422 (2013)
11. Dabov, K., Foi, A., Katkovnik, V., Egiazarian, K.: Image denoising by sparse 3-D transform-domain collaborative filtering. IEEE Trans. Image Process **16**(8), 2080–2095 (2007)
12. Danielyan, A., Katkovnik, V., Egiazarian, K.: BM3D frames and variational image deblurring. IEEE Trans. Image Process **21**(4), 1715–1728 (2012). https://doi.org/10.1109/TIP.2011.2176954
13. Ding, D., Ram, S., Rodríguez, J.J.: Image inpainting using nonlocal texture matching and nonlinear filtering. IEEE Trans. Image Process **28**(4), 1705–1719 (2018)
14. Durand, S., Fadili, J., Nikolova, M.: Multiplicative noise removal using L1 fidelity on frame coefficients. J. Math. Imaging Vision **36**(3), 201–226 (2010)
15. Elharrouss, O., Almaadeed, N., Al-Maadeed, S., Akbari, Y.: Image inpainting: a review. Neural Process. Lett. pp. 1–22 (2019)
16. Fu, S., Zhang, C., Tai, X.: Image denoising and deblurring: nonconvex regularization, inverse diffusion and shock filter. Sci. China Inf. Sci. **54**(6), 1184–1198 (2011)
17. Gilboa, G., Osher, S.: Nonlocal linear image regularization and supervised segmentation. Multiscale Modeling Simul. **6**(2), 595–630 (2007)
18. Gilboa, G., Osher, S.: Nonlocal operators with applications to image processing. Multiscale Modeling Simul. **7**(3), 1005–1028 (2008)
19. Hajiaboli, M.R.: A self-governing hybrid model for noise removal. In: Pacific-Rim symposium on image and video technology, pp. 295–305. Springer (2009)
20. Hajiaboli, M.R.: An anisotropic fourth-order diffusion filter for image noise removal. Int. J. Comput. Vision **92**(2), 177–191 (2011)
21. Holla Kayyar, S., Jidesh, P.: Non-local total variation regularization approach for image restoration under a poisson degradation. J. Mod. Opt. **65**(19), 2231–2242 (2018)
22. Hou, G., Pan, Z., Wang, G., Yang, H., Duan, J.: An efficient nonlocal variational method with application to underwater image restoration. Neurocomputing **369**, 106–121 (2019). https://doi.org/10.1016/j.neucom.2019.08.041. (www.sciencedirect.com/science/article/pii/S0925231219311798)
23. Jin, Y., Jiang, X., Jiang, W.: An image denoising approach based on adaptive nonlocal total variation. J. Vis. Commun. Image Represent. **65**, 102661 (2019). https://doi.org/10.1016/j.jvcir.2019.102661. (www.sciencedirect.com/science/article/pii/S1047320319302822)
24. Jung, M., Bresson, X., Chan, T.F., Vese, L.A.: Nonlocal Mumford-Shah regularizers for color image restoration. IEEE Trans. Image Process. **20**(6), 1583–1598 (2010)
25. Karami, F., Meskine, D., Sadik, K.: A new nonlocal model for the restoration of textured images. J. Appl. Anal. Comput. **9**(6), 2070–2095 (2019)
26. Karami, F., Sadik, K., Ziad, L.: A variable exponent nonlocal p(x)-laplacian equation for image restoration. Comput. Math. Appl. **75**(2), 534–546 (2018). https://doi.org/10.1016/j.camwa.2017.09.034. (www.sciencedirect.com/science/article/pii/S0898122117305977)
27. Kim, S., Lim, H.: Fourth-order partial differential equations for effective image denoising. Electron. J. Differ. Equ. **17**, 107–121 (2009)
28. Laghrib, A., Ghazdali, A., Hakim, A., Raghay, S.: A multi-frame super-resolution using diffusion registration and a nonlocal variational image restoration. Comput. Math. Appl. **72**(9), 2535–2548 (2016). https://doi.org/10.1016/j.camwa.2016.09.013. (www.sciencedirect.com/science/article/pii/S0898122116305259)
29. Li, F., Pi, L., Zeng, T.: Explicit coherence enhancing filter with spatial adaptive elliptical kernel. IEEE Signal Process. Lett. **19**(9), 555–558 (2012)
30. Li, P., Li, S.J., Yao, Z.A., Zhang, Z.J.: Two anisotropic fourth-order partial differential equations for image inpainting. IET Image Proc. **7**(3), 260–269 (2013)
31. Liu, Q., Gao, X., He, L., Lu, W.: Single image dehazing with depth-aware non-local total variation regularization. IEEE Trans. Image Process **27**(10), 5178–5191 (2018). https://doi.org/10.1109/TIP.2018.2849928
32. Liu, Q., Zhang, Z., Guo, Z.: On a fractional reaction-diffusion system applied to image decomposition and restoration. Comput. Math. Appl. **78**(5), 1739–1751 (2019). https://doi.org/10.1016/j.camwa.2019.05.030. (www.sciencedirect.com/science/article/pii/S0898122119302937. AdvancesinFractionalDifferentialEquations(V):Time-spacefractionalPDEs)
33. Liu, X., Chen, Y.: NLTV-Gabor-based models for image decomposition and denoising. SIViP **14**(2), 305–313 (2020). https://doi.org/10.1007/s11760-019-01558-6.
34. Lou, Y., Zhang, X., Osher, S., Bertozzi, A.: Image recovery via nonlocal operators. J. Sci. Comput. **42**(2), 185–197 (2010)

35. Lv, X.G., Song, Y.Z., Wang, S.X., Le, J.: Image restoration with a high-order total variation minimization method. Appl. Math. Model. **37**(16), 8210–8224 (2013). https://doi.org/10.1016/j.apm.2013.03.028. (www.sciencedirect.com/science/article/pii/S0307904X13001832)
36. Lysaker, M., Lundervold, A., Tai, X.C.: Noise removal using fourth-order partial differential equation with applications to medical magnetic resonance images in space and time. IEEE Trans. Image Process. **12**(12), 1579–1590 (2003)
37. Ma, X., Shen, H., Zhao, X., Zhang, L.: Sar image despeckling by the use of variational methods with adaptive nonlocal functionals. IEEE Trans. Geosci. Remote Sens. **54**(6), 3421–3435 (2016). https://doi.org/10.1109/TGRS.2016.2517627
38. Newson, A., Almansa, A., Gousseau, Y., Pérez, P.: Non-local patch-based image inpainting. Image Process. Line **7**, 373–385 (2017)
39. Nie, X., Qiao, H., Zhang, B., Huang, X.: A nonlocal tv-based variational method for polsar data speckle reduction. IEEE Trans. Image Process **25**(6), 2620–2634 (2016). https://doi.org/10.1109/TIP.2016.2552402
40. Papyan, V., Elad, M.: Multi-scale patch-based image restoration. IEEE Trans. Image Process **25**(1), 249–261 (2016). https://doi.org/10.1109/TIP.2015.2499698
41. Perona, P., Malik, J.: Scale-space and edge detection using anisotropic diffusion. IEEE Trans. Pattern Anal. Mach. Intell. **12**(7), 629–639 (1990)
42. Rudin, L.I., Osher, S., Fatemi, E.: Nonlinear total variation based noise removal algorithms. Phys. D **60**(1–4), 259–268 (1992)
43. Schönlieb, C.B.: Partial differential equation methods for image inpainting. Cambridge University Press, Cambridge (2015). https://doi.org/10.1007/s11760-019-01558-6
44. Shah, J.: A common framework for curve evolution, segmentation and anisotropic diffusion. In: Proceedings CVPR IEEE computer society conference on computer vision and pattern recognition, pp. 136–142. IEEE (1996)
45. Takeda, H., Farsiu, S., Milanfar, P.: Deblurring using regularized locally adaptive kernel regression. IEEE Trans. Image Process. **17**(4), 550–563 (2008)
46. Wan, W., Liu, J.: Nonlocal patches based Gaussian mixture model for image inpainting. Appl. Math. Model. **87**, 317–331 (2020). https://doi.org/10.1016/j.apm.2020.05.030. (www.sciencedirect.com/science/article/pii/S0307904X20302705)
47. Wang, Z., Bovik, A.C., Sheikh, H.R., Simoncelli, E.P.: Image quality assessment: from error visibility to structural similarity. IEEE Trans. Image Process. **13**(4), 600–612 (2004)
48. Wen, Y., Vese, L.A.: Nonlocal adaptive biharmonic regularizer for image restoration. In: International symposium on visual computing, pp. 670–681. Springer (2020)
49. Wen, Y.W., Ng, M.K., Ching, W.K.: Iterative algorithms based on decoupling of deblurring and denoising for image restoration. SIAM J. Sci. Comput. **30**(5), 2655–2674 (2008)
50. Xu, J., Feng, A., Hao, Y., Zhang, X., Han, Y.: Image deblurring and denoising by an improved variational model. AEU-Int. J. Electron. C. **70**(9), 1128–1133 (2016). https://doi.org/10.1016/j.aeue.2016.05.008. (www.sciencedirect.com/science/article/pii/S1434841116301704)
51. Yao, W., Guo, Z., Sun, J., Wu, B., Gao, H.: Multiplicative noise removal for texture images based on adaptive anisotropic fractional diffusion equations. SIAM J. Imag. Sci. **12**(2), 839–873 (2019)
52. You, Y.L., Kaveh, M.: Fourth-order partial differential equations for noise removal. IEEE Trans. Image Process. **9**(10), 1723–1730 (2000)
53. Yu, J., Lin, Z., Yang, J., Shen, X., Lu, X., Huang, T.S.: Generative image inpainting with contextual attention. In: Proceedings of the IEEE conference on computer vision and pattern recognition, pp. 5505–5514 (2018)
54. Zhang, J., Chen, K.: A total fractional-order variation model for image restoration with nonhomogeneous boundary conditions and its numerical solution. SIAM J. Imag. Sci. **8**(4), 2487–2518 (2015)

Ying Wen received her Ph.D. degree in computational mathematics from Harbin Institute of Technology, Harbin, China, in 2022. From September 2019 to October 2020, she worked with Professors Andrea Bertozzi and Luminita Vese as a visiting student at UCLA. Her research interests include partial differential equations and image restoration.

Luminita A. Vese received the M.S. degree in mathematics from West University of Timisoara, Romania, in 1993, and the M.S. and Ph.D. degrees in applied mathematics from University of Nice, Sophia, Antipolis, France, in 1992 and 1997, respectively. She is currently a Professor of Mathematics at the University of California, Los Angeles (UCLA). Before joining the UCLA faculty, she held postdoctoral research and teaching positions at the University of Nice, the University of Paris IX Dauphine, and UCLA. Her research interests include variational methods and partial differential equations, inverse problems, image analysis, and computer vision.

Kehan Shi received the Ph.D. degree from Harbin Institute of Technology, Harbin, China, in 2018. He is currently a Lecturer in the Department of Mathematics, China Jiliang University, Hangzhou, China. His research interests include nonlinear diffusion equations and mathematical image processing.

Zhichang Guo received his Ph.D. degree from Jilin University, Changchun, China, in 2010. He is currently an associate professor at School of Mathematics, Harbin Institute of Technology, Harbin, China. His research interests include partial differential equations, nonlinear analysis, mathematical methods in image analysis, and deep learning.

Jiebao Sun received his Ph.D. degree from Jilin University, Changchun, China, in 2008. He is currently a professor at School of Mathematics, Harbin Institute of Technology, Harbin, China. His research interests include partial differential equations, nonlinear diffusion, and mathematical methods in image analysis.